Available online at www.sciencedirect.com

ScienceDirect

Advances in Space Research 73 (2024) 2685–2702

ADVANCES IN SPACE RESEARCH
(a COSPAR publication)

www.elsevier.com/locate/asr

Paleoenvironmental significance of Fe/Mg phyllosilicate and sulfate deposits in Mikumi crater, northern Meridiani Planum, Mars

Beatrice Baschetti [a,b,c,*], Alessandro Frigeri [b], Francesca Altieri [b], Cristian Carli [b], Adriano Tullo [d], Maria Sgavetti [e]

[a] *Università degli studi di Padova, Department of Geosciences, Via G. Gradeningo 6, Padova 35131, Italy*
[b] *INAF/IAPS, Via del Fosso del Cavaliere 100, Rome 00133, Italy*
[c] *Sapienza Università di Roma, Department of Physics, p.le Aldo Moro 2, Rome 00185, Italy*
[d] *INAF/OAPd, Vicolo dell'Osservatorio, 5, Padova 35122, Italy*
[e] *Università degli Studi di Parma, Department of Chemistry, Parco Area delle Scienze 17/A, Parma 43124, Italy*

Received 20 November 2023; accepted 28 December 2023
Available online 3 January 2024

Abstract

The region of Meridiani Planum on Mars retains the evidence of multiple surface and near-surface aqueous processes that span from the Noachian to the Hesperian. This makes it an interesting spot for better understanding the characteristics and the evolution of Mars' aqueous environment between these two fundamental epochs. Here we investigate the mineralogy, stratigraphy, and morphology of the Noachian–Hesperian sedimentary materials that fill a 16-km-wide crater named Mikumi, located in the northern part of Meridiani Planum. The analysis was carried out combining observations from the Compact Reconnaissance Imaging Spectrometer for Mars (CRISM), the High Resolution Imaging Science Experiment (HiRISE), and the Context Imager (CTX). About 20–30 meters, on average, of Fe/Mg phyllosilicate-rich rocks and a thick sequence (75 m) of both mono- and polyhydrated Mg sulfates are detected on the crater floor. Both layers postdate the impact event. Most of the hydrated terrains are extensively polygonally fractured, suggesting the possible action of water-related processes such as desiccation and hydro fracturing on the sediments. Stratigraphic analysis clearly shows that Fe/Mg phyllosilicates were deposited on top of the sulfate sequence, meaning that they are younger than sulfates. This can have interesting implications on paleoclimatic studies of Mars as it shows that a simple timeline going from a clay-rich Noachian to a sulfate-rich Hesperian oversimplifies the evolution of Mars' mineralogy and related aqueous environment at the Noachian–Hesperian boundary.

Keywords: Mars; Mineralogy; Spectroscopy; Remote Sensing; Hyperspectral Imaging; Stratigraphy; Paleoclimate

1. Introduction

Meridiani Planum is a relatively flat area of Mars located south-west of Arabia Terra and approximately extending from longitude 350°E to 10°E and latitude −5°N to 10°N. The region retains evidence of a complex geological history, including a succession of different paleoenvironments from Early Noachian to Late Hesperian (Hynek et al., 2017), which represent a rich and varied record of Mars' past surface conditions. In particular, orbital data indicates that Meridiani Planum hosts a thick sequence of sedimentary rocks (Arvidson et al., 2003), where hematite, sulfates, and phyllosilicates (clay minerals) are detected (Christensen et al., 2001; Poulet et al., 2008;

* Corresponding author at: Università degli studi di Padova, Department of Geosciences, Via G. Gradeningo 6, Padova 35131, Italy.
E-mail addresses: beatrice.baschetti@inaf.it (B. Baschetti), alessandro.frigeri@inaf.it (A. Frigeri), francesca.altieri@inaf.it (F. Altieri), cristian.carli@inaf.it (C. Carli), adriano.tullo@inaf.it (A. Tullo), maria.sgavetti@unipr.it (M. Sgavetti).

https://doi.org/10.1016/j.asr.2023.12.060
0273-1177/

Wiseman et al., 2010; Flahaut et al., 2015). In January 2004, the NASA's Mars Exploration Rover-B (MER-B) Opportunity landed in Meridiani Planum in order to explore part of this sequence. The rover operated for more than 14 years, investigating the geochemistry and mineralogy of outcrops, soils, and loose rocks at the surface, along with carrying out sedimentologic and stratigraphic analyses. Both orbital and in situ data support the existence of prolonged surface and near-surface water activity in the region: this makes Meridiani Planum a key area to retrieve information on Mars' ancient climate and habitability.

1.1. Geologic context

Based on the geologic map at scale 1:2,000,000 by Hynek et al. (2017) (Fig. 1a), we list here the main geologic units of Meridiani Planum along with a short description:

(a) Nhc1 and Nhc2: these units are also referred to as subdued cratered unit (Nhc1) and cratered unit (Nhc2). Their age is estimated around the Early/Middle Noachian and they are the oldest preserved crust in this area. Especially on Nhc1, which is the oldest of

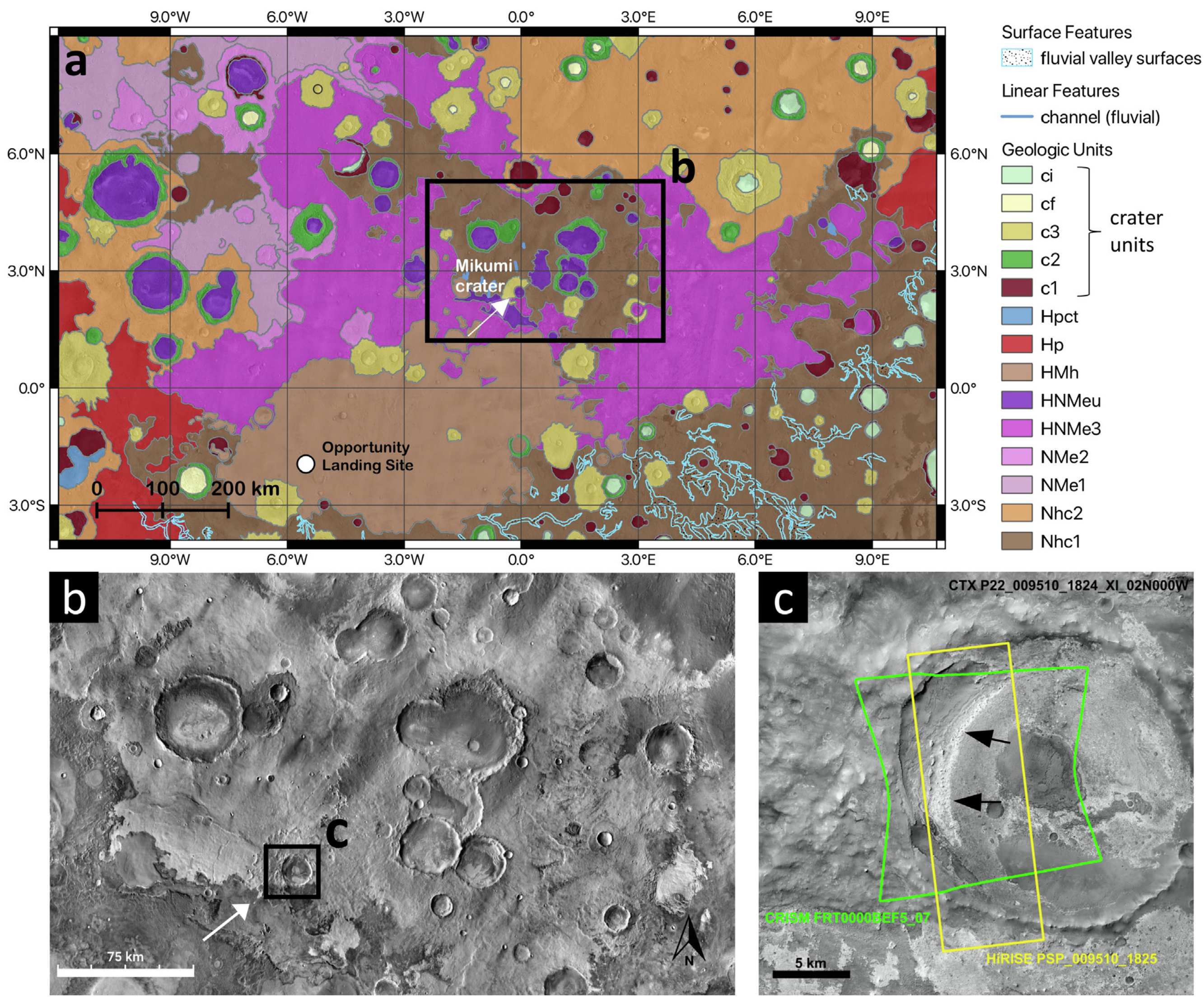

Fig. 1. (a) Geologic map of Meridiani Planum, modified after Hynek et al. (2017). Geologic units are described in Section 1.1. The location of Mikumi crater is pointed at by a white arrow. (b) Thermal Emission Imaging System (THEMIS) daytime image of the terrains surrounding Mikumi crater (white arrow). The area shown here is mainly part of the Noachian-aged geological unit exposed in northern Meridiani Planum (Nhc1); (c) CTX (P22_009510_1824_XI_02N000W) of Mikumi's floor and part of its ejecta, CRISM and HiRISE footprints used in this study are superimposed on the image. Two black arrows point at the brighter deposits inside the western part of the crater, along which a scarp exposes the layers of sedimentary materials which fill the crater floor.

the two, Hynek et al. (2017) observe several erosional features formed by fluvio-lacustrine activity such as valley network systems, crater floor deposits and heavily degraded crater rims.

(b) NMe1, NMe2, HNMe3, and HNMeu: globally termed as etched units. Their age ranges between Late Noachian and Early Hesperian and they were unconformably emplaced on the cratered and subdued cratered units in a distinct deposition environment that postdates the valley network activity. The etched units are composed of an easily erodible material whose origin is still debated (Hynek et al., 2019, and references therein) and which was probably much more extensive in the past, completely covering the underlying Nhc1 and Nhc2 units. Subsequent erosion of the deposited material led to resurfacing in some areas (Zabrusky et al., 2012), leaving some remnant deposits mainly inside impact craters.

(c) HMh: also referred to as hematite unit. The age of this unit is estimated to be around Early Hesperian. HMh superposes the etched units, constituting the top layer of most of the southern part of Meridiani Planum. In situ observations by Opportunity show that it is mainly composed by hematite under the form of spherules measuring ~ 1–5 mm in diameter and concentrated as an aeolian lag deposit (Squyres et al., 2004; Arvidson et al., 2006). Hematite was first detected from orbit by Christensen et al. (2001), leading to the choice of the area for the landing of the NASA rover.

(d) Hp or plains unit (Hesperian): this unit was emplaced right after the hematite plains, filling topographic lows and overlying all the previously described units. Due to some of its features, such as lobate margins, Hynek et al. (2017) suggest Hp originated from low-viscosity lava flows, although the signs of volcanic eruptions that supplied the lava are not visible.

(e) Hpct or chaotic unit (Late Hesperian): this unit is present only in the southwestern part of the area and it's part of Iani Chaos region located west of Meridiani Planum. The deposits have the typical characteristics of chaotic deposits on Mars, composed by heavily fractured materials.

1.2. Aqueous activity in Meridiani Planum

Multiple evidence shows that Meridiani Planum was once extensively characterised by surface and near-surface aqueous activity, and that surface conditions probably varied multiple times between the Noachian and the Hesperian. First, the oldest exposed geological units (Nhc1 and Nhc2) consist of heavily cratered Noachian-aged terrains, where several channels and valley networks have left their traces on the surface (Hynek et al., 2010; Hynek et al., 2017; Williams et al., 2017). Regional differences in the morphology of the valley networks also suggest some temporal changes in aqueous processes with an early phase of high water runoff and later phases associated to groundwater processes and local dissolution that reactivated some of the valley networks (Williams et al., 2017). The bedrock exposed in Nhc1 and Nhc2 is rich in mafic components (e.g. Griffes et al., 2007; Poulet et al., 2008) but with sparse hydration features (e.g. Poulet et al., 2008; Flahaut et al., 2015), the latter usually found inside craters. Secondly, the etched units (NMe1, NMe2, HNMe3, and HNMeu) retain orbital (e.g. Poulet et al., 2008; Wiseman et al., 2010; Flahaut et al., 2015) and in situ evidence (e.g. Clark et al., 2005; Squyres et al., 2006) for hydrated minerals such as phyllosilicates and abundant sulfates: both these minerals usually form by alteration in aqueous environments. The Opportunity team, who mainly explored the hematite unit and the upper sequence of the underlying etched unit, also found morphological evidence consistent with episodic inundations, followed by evaporation and desiccation, suggesting the existence of a playa or sabkha environment (Squyres et al., 2004). Finally, several karsts features, such as dolines and pans, are observed with varying density degrees on the hydrated etched terrains and might indicate the action of both surficial water and groundwater in this area after the sedimentation of the etched units (Baioni and Sgavetti, 2013; Flahaut et al., 2015).

1.3. Objectives and motivation

Thanks to its distinctive characteristics and also due to Opportunity's exploration campaign, many studies have focused on Meridiani Planum trying to understand the geology, stratigraphy and composition of the units in this area, especially the etched units and the hematite unit. However, remnants of the etched units, classified as HNMeu by Hynek et al. (2017), are also scattered on Nhc1 and Nhc2 units, usually inside craters, where they show very interesting and rather complex sedimentary structures, with signs of hydrated mineralogy (e.g. Poulet et al., 2008). A valuable test case to study the HNMeu materials is provided by a small crater named Mikumi, which is located within the northern part of Meridiani Planum, centered at 359.96°E, 2.45°N (Figs. 1a, 1b, and 1c). The crater has a diameter of 16 km and is embedded within the Noachian-aged subdued cratered unit (Nhc1) defined by Hynek et al. (2017), which in this area approximately extends from latitude 1°N to 7°N and from longitude 355°E to 4°E. In particular, Mikumi is located along the southern border of the unit (Fig. 1a and 1b). The floor of Mikumi crater is filled by HNMeu sedimentary materials showing an asymmetrical distribution, with some brighter deposits on the western part (Fig. 1c, black arrows); here a scarp exposes the layers of these sediments and gives us the opportunity to study them in detail. In this study we carry out a mineralogical, stratigraphic, and morphological investigation of Mikumi crater focusing on the characterization of these sedimentary infillings with several instruments onboard NASA's Mars Reconnaissance Orbiter (MRO) (Zurek and Smrekar, 2007). In particular, we use spectral data from the Compact Reconnaissance Imaging Spectrometer for Mars (CRISM) (Murchie et al., 2007) and high resolution camera data from the High Resolution Imaging Science Experiment (HiRISE) (McEwen et al., 2007). Data from the Context Imager (CTX) (Malin et al., 2007) camera are also used to explore the general context of the crater floor and its ejecta.

2. Datasets and Methods

2.1. Hyperspectral data

The information on the mineralogical composition of Mikumi crater is retrieved using CRISM FRT0000BEF5_07 Targeted Reduced Data Record (TRR), acquired on 6 August 2008 with full spectral (6.55 nm/channel) and spatial resolution (15–19 m/pixel). The dataset covers the west part of the crater's terrains, including part of the rim (Fig. 1c, as shown by the green outline). There are a few other CRISM Targeted images that cover part of Mikumi crater and/or its surroundings, among which there is one (FRT000012ABB_07) that is almost perfectly superimposed to FRT0000BEF5_07. We also analysed this second image and were able to obtain the same results we had got from FRT0000BEF5_07. For this reason, we will be showing here the results from FRT0000BEF5_07 only, while the analysis of FRT000012ABB_07 is available in the Supplementary Materials. Other targeted images nearby were not included as they mainly cover Mikumi's ejecta and can be of minimal support for studying the sediments on the crater floor, which is our main objective in this study.

The relevant wavelengths for our analysis are between 1.0 and 4.0 μm, we therefore focus on the L (infrared) part of the CRISM dataset. This wavelength range is commonly used for mineralogical analysis on Mars as it retains the key spectral features (Viviano-Beck et al., 2014) for identifying: (a) primary rock-forming minerals, like for example olivine and pyroxenes, based on their crystal field absorptions (e.g. Burns, 1993; Poulet et al., 2008); (b) secondary minerals, like those formed by processes such as aqueous alteration, considering their overtone absorptions (e.g. Clark et al., 1990; Bibring et al., 2006).

The dataset is processed using the CRISM Analysis Toolkit (CAT) tool on ENVI® software (L3HARRIS™) and corrected for atmospheric absorption with the "volcano-scan" method (McGuire et al., 2009). We use the reflectance factor, hereafter reflectance, as a unit for the final product. We also further processed the spectral cube so that each pixel is ratioed to a reference spectrum from the same detector column in order to mitigate column-dependent instrumental effects and emphasise the spectral features of interest. The reference spectrum should be ideally neutral, with no distinctive absorption features. In our case, we use a reference spectrum which is obtained by computing the median of all the spectra with no features of specific mineralogy within the column.

We explore the overall composition of the crater's terrains using CRISM spectral parameters and browse products from Viviano-Beck et al. (2014). In particular, we focus on the mafic and hydrated mineralogy, using the MAF and HYD browse products. The hydrated mineralogy is also further explored with BD1900R2 and BD2290 spectral parameters.

(a) The MAF ("mafic mineralogy") browse product shows information related to mafic mineralogy. It combines the three spectral parameters OLINDEX3, LCPINDEX2 and HCPINDEX2. OLINDEX3 is sensitive to olivine, detecting its broad absorption at 1 μm. This absorption is caused by the presence of iron in the two octahedral sites of the mineral (M1 and M2). The presence of iron in M1 and M2 generates three close absorptions, which result in a wide composite absorption around 1 μm in the spectrum (Burns, 1993). With increasing iron abundance, the absorption moves to longer wavelengths (e.g. Burns, 1993; Sunshine and Pieters, 1998; Isaacson et al., 2014). LCPINDEX2 and HCPINDEX2 reveal the presence of pyroxenes, respectively low calcium and high calcium. Several pyroxenes have a broad absorption around 1 and 2 μm deriving from crystal field transitions of Fe^{2+} (Burns, 1993). For low-Ca pyroxenes, this absorption, together with the one around 1 μm, shifts from shorter to longer wavelengths with increasing Fe^{2+}/Mg^{2+} content (e.g. Klima et al., 2007). Increasing Ca in the M2 octahedral site further moves both bands at longer wavelengths (see for example Cloutis and Gaffey, 1991; Klima et al., 2011; Viviano-Beck et al., 2014).

(b) The HYD ("hydrated mineralogy") browse product shows information about structurally bound water in minerals. It combines the three spectral parameters SINDEX2, BD2100_2 and BD1900_2. SINDEX2 detects the convexity at 2.29 μm due to 2.1 and 2.4 μm absorptions caused by water-related vibrations typical of several sulfate minerals (Clark et al., 1999). In particular, polyhydrated sulfates display a 2.4 μm feature due to water combinations and/or overtones, while monohydrated sulfates display both a 2.1 and a 2.4 μm feature, with the 2.1 μm feature caused by H_2O vibrational combinations that shift to longer wavelengths for Mg cations (e.g. Mg-kieserite) with respect to Fe cations (e.g. Fe-szomolnokite) (Viviano-Beck et al., 2014; Cloutis et al., 2006). BD2100_2 detects the previously mentioned 2.1 μm H_2O band depth in monohydrated sulfates and BD1900_2 detects the 1.9 μm H_2O band depth typical of many hydrated minerals such as clays, carbonates and sulfates.

(c) In addition to that, we also explore BD1900R2 and BD2290 spectral parameters. BD1900R2, similarly to BD1900_2, marks the 1.9 μm H_2O absorption feature, while BD2290 quantifies the depth of the 2.29 μm feature caused by metal-OH vibrations in Mg, Fe-OH minerals such as Fe/Mg smectites.

CRISM spectral parameters and browse products are extremely useful for a quick assessment of the spectral variability of the surface. However, the mineralogy suggested by these techniques needs to be verified by directly looking at the spectra from the evidenced areas (see Section 3). In order to maintain the correspondence between the pixels of each column, the whole spectral analysis is carried out using the sensor space data, however, for graphical purposes, we will show the georeferenced version of the figures obtained from the dataset.

2.2. Camera data

The morphological aspects of Mikumi crater are investigated using CTX and HiRISE data. CTX data have a spatial resolution of 6 m/pixel (Malin et al., 2007) and are used to study the main morphological features of the crater, as well as to perform mapping and produce a DTM. The DTM was created through the NASA ASP and USGS ISIS pipeline by stereogrammetry on CTX images P22_009510_1824 and P03_002113_1825, and the resulting model was aligned to MOLA. With plane fitting against the elevation model, we were able to measure the dip of the layered sediments within Mikumi. This technique carries an important degree of uncertainty and variability, however, repetition over a statistically significant number of samples is able to provide an overall average trend. CTX data are also used, along with Thermal Emission Imaging System (THEMIS) daytime data, to give surrounding context to the crater (Fig. 1c), and to check its stratigraphic position relative to the several geologic units in the area. The small-scale morphology is investigated through HiRISE PSP_ 009510_1825_RED and PSP_ 009510_1825_MRGB products, which have a spatial resolution of 0.25 m/pixel and are acquired using the red, and red plus blue-green filter respectively (McEwen et al., 2007). Like the CRISM dataset, these HiRISE products cover the western crater's deposits and part of the rim, providing high-resolution coverage for a good part of the area imaged by CRISM (Fig. 1c).

3. Mineralogical characterization

As stated in the introduction, previous works have pointed out that the northern part of Meridiani Planum (Nhc1 and Nhc2 units) appears to be dominated mainly by pyroxenes (e.g. Griffes et al., 2007; Poulet et al., 2008), with signs of Fe/Mg phyllosilicates usually inside craters (e.g. Poulet et al., 2008; Flahaut et al., 2015). We therefore test the mafic mineralogy through the MAF browse product and the hydrated mineralogy through the HYD browse product and BD1900R2-BD2290 spectral parameters. We list here the different mineralogies identified within the crater's terrains (Fig. 2). All the displayed spectra come from the ratioed cube obtained with the procedure described in Section 2.1. For the spectra location and a complete explanation of selection methods see the Supplementary Materials.

(a) **Low-calcium pyroxenes**. Low-Ca pyroxenes (associated to the LCPINDEX2 spectral parameter) are found on the rim of the crater and the areas outside it (Figure S8); these terrains are shown in red in Fig. 2b. The wider pyroxene-rich area corresponds to the upper left part of the CRISM image but smaller deposits are also visible in the bottom left part. The spectra extracted are characterised by a broad absorption around 2 μm, as it can be seen in the red spectrum in Fig. 2d, which is the result of the mean of several spectra in the northwestern area (Table S3). The other two mafic spectral parameters, HCPINDEX2 and OLINDEX3, couldn't identify an equally conclusive and strong signature.

(b) **Mono- and polyhydrated sulfates**. Focusing on the crater's floor, the HYD browse product (Fig. 2c) highlights many areas where spectra show signs of hydration as a major feature. Yellow and magenta areas respectively indicate the presence of mono- and polyhydrated sulfates (Figure S8), while blue areas are indicative of the presence of other hydrated minerals such as clays or carbonates. We extract two mean spectra from yellow and magenta areas using the polygonal ROI feature on ENVI® (Figure S7). The extracted spectra confirm the presence of sulfate minerals and are shown in magenta and orange in Fig. 2d. The orange spectrum shows a broad absorption in the 1.9–2.15 μm area with two minima at 1.925 and 2.123 μm and two other absorption features at longer wavelengths, one at 2.4 μm and one at 2.525 μm. These features are compatible with kieserite. The magenta spectrum has absorption features at 1.4, 1.9 and 2.4 μm and we interpret this as indicative of the presence of polyhydrated sulfates (Mg-sulfate). The laboratory spectra of the sulfates we use for comparison are shown in Fig. 2e with the same colour code and are taken from the RELAB database.

(c) **Fe/Mg phyllosilicates**. We now focus on the remaining hydrated mineralogy, which is shown in blue in the HYD browse product in Fig. 2c. We do that with the aid of BD1900R2 and BD2290 parameters. The custom browse product shown in Fig. 2b highlights two different regions, depending on the values of the two parameters: blue regions indicate areas that match with the BD1900R2 parameter but do not match with BD2290, while aquamarine regions indicate areas matching with both BD1900R2 and BD2290. We extract a representative spectrum of

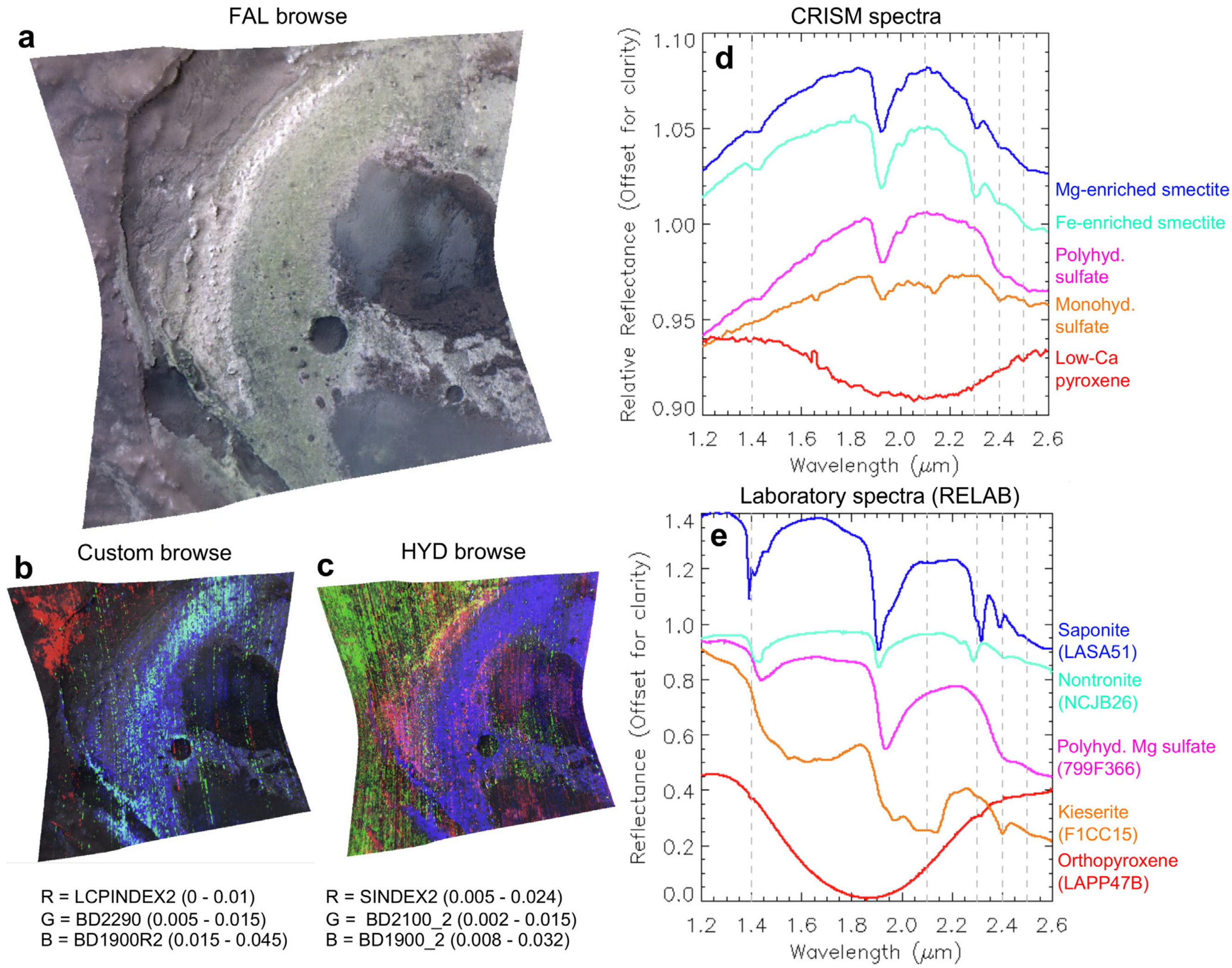

Fig. 2. (a) CRISM enhanced infrared image of the area analysed (FAL browse product). R = reflectance at 1.15 μm, G = reflectance at 1.50 μm and B = reflectance at 2.52 μm. The wavelengths are chosen to highlight differences between key mineral groups: red/orange colours are usually characteristic of olivine-rich material, blue/green often indicate clay, green may also indicate carbonate, and grey/brown often indicate mafic material; (b) CRISM custom browse product. Red areas show a strong low-Ca pyroxene component, blue areas indicate Mg-richer smectites, while aquamarine areas indicate Fe-richer smectites. The three parameters that have been used for this custom RGB composite are: LCPINDEX2, BD2290, BD1900R2. Their explicit range values are listed in the figure. (c) CRISM HYD browse product. Yellow areas are indicative of monohydrated sulfates, while magenta areas indicate polyhydrated sulfates. Blue areas highlight the presence of other hydrated materials such as clays or carbonates. The three parameters that have been used for the HYD RGB composite are: SINDEX2, BD2100_2, and BD1900_2, explicit range values are listed in the figure. (d) CRISM spectra of detected mineralogy. (e) Laboratory spectra of minerals which match with the CRISM spectra.

each area algorithmically, selecting only pixels within specific ranges of the two spectral parameters. A detailed explanation and explicit values are reported in the Supplementary Materials (Figures S1-S3, and tables S1-S2). The results are displayed in Fig. 2d. Both the spectra obtained show absorption features at ~1.4 μm (OH vibrations), ~ 1.9 μm (OH and H-O–H vibrations), ~ 2.3 μm and ~ 2.4 μm (metal-OH vibrations), which are compatible with the presence of Fe/Mg phyllosilicates (Fe/Mg smectites). The 1.4 μm feature is centered around 1.43 μm for both spectra. Interestingly, for the 2.3 μm band, the aquamarine spectrum has a deeper minimum centered around 2.305 μm, while the blue spectrum has it centered around 2.315 μm (Fig. 2d and 3a). The shift at longer wavelengths and the lowest intensity of the 2.3 μm feature in the blue spectrum explain why the BD2290 parameter has much lower values in the blue unit with respect to the aquamarine unit. At 2.4 μm the two spectra have similar bands with no evident shift. Finally, a weak 2.52 μm feature appears in both spectra, although slightly more evident for the aquamarine spectrum. The depth of this feature is comparable to noise levels, for this reason it is not further discussed. Laboratory spectra of Fe/Mg-phyllosilicates are shown for comparison in Fig. 2e. Details of the absorption features in the 2.2–2.6 μm range are then shown in Fig. 3. In Fe/Mg-bearing

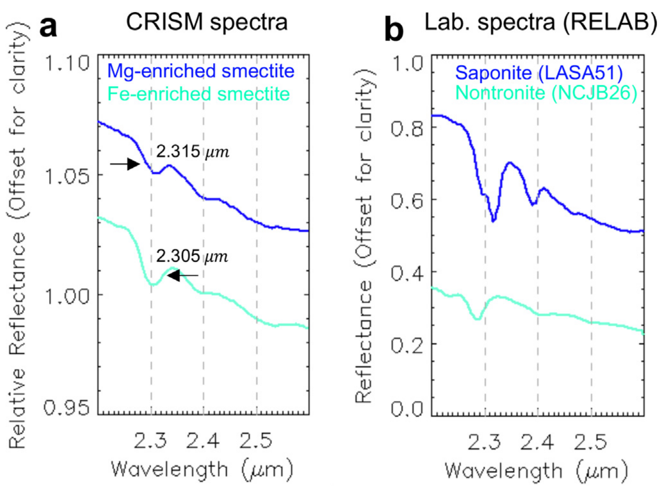

Fig. 3. (a) Detail of the wavelength range 2.2–2.6 μm for the spectra of Fe/Mg phyllosilicates shown in Fig. 2d. Blue is for Mg-richer smectites, aquamarine is for Fe-richer smectites. Notice the shift towards longer wavelengths for the 2.3 μm absorption in the blue spectrum, where the band center is at 2.315 μm, while we have a 2.305 μm band center for the aquamarine spectrum. The shift is indicative of the different Fe/Mg cation abundance in the two clay minerals. Overtones at 2.4 and 2.5 μm are also slightly visible; (b) Laboratory spectra of saponite (Mg-rich phyllosilicate) and nontronite (Fe-rich) used for comparison with CRISM spectra.

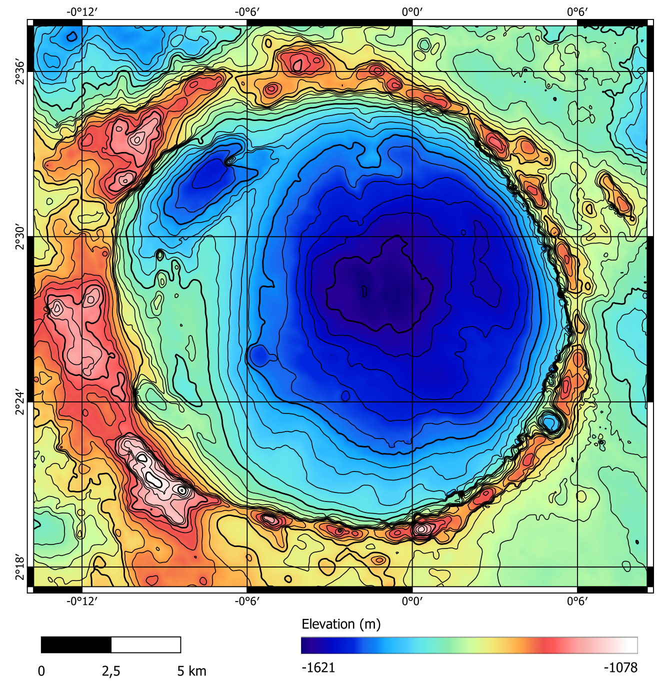

Fig. 4. Topographic map of Mikumi crater. Isolines are spaced by 25 meters. Surface elevation relative to the Martian datum.

phyllosilicates the 2.3 μm feature shifts to longer wavelengths as Mg is exchanged for Fe (Clark et al., 1990). Therefore, based on the position of the 2.3 μm overtone, we suggest that in blue areas smectites are more enriched in Mg (2.315 μm band center), while in aquamarine areas they have less Mg content and more Fe (band centered at 2.305 μm).

It is important to note that CRISM data show the spectrally dominant phases which are present in each pixel of the dataset and that they can be influenced by other phases present in the regions analysed. Moreover, they have a lower spectral resolution with respect to laboratory data. As a consequence, the spectral features observed are generally weaker and do not perfectly coincide in shape and position with the ones from laboratory spectra.

4. Morphology

Mikumi crater is situated within Noachian terrains in the northern part of Meridiani Planum (Nhc1 unit) and its ejecta are partially covered to the south by the etched deposits (Hynek et al. (2017); Fig. 1a and 1b), which are rich in sulfates and clays (Flahaut et al., 2015). The valley network activity in the area predates the formation of the crater as its ejecta overlies several channels carved on the Noachian bedrock (Williams et al., 2017).

The floor of Mikumi crater retains a certain degree of asymmetry, as we can see from the topography in Fig. 4, with the lowest part decentralised towards north-east. A smaller low area is also located in the north-west. The crater rim shows some levels of asymmetry as well, with the western side reaching a mean altitude of -1200 m and the eastern side settling between -1250 m and -1300 m. Such difference may either be a result of the inclination of the impact, although the crater doesn't show signs of ellipticity, or the result of differential erosion. The distribution of the topography of the surrounding area is antithetical to that of the rim, generally higher in the eastern zone. The crater floor is mainly filled by sedimentary materials which correspond to the clay and sulfate-bearing units identified in the spectral analysis (Fig. 2b, 2c). A scarp that runs along almost the whole western part of the crater exposes the layers of the sediments. According to the total depth-diameter relationship (d_t/D) derived in Mouginis-Mark et al. (2018), a diameter of about 16 km corresponds to an original depth, prior to the crater's infilling and degradation, between 2.2 and 3.6 km. Conversely, the maximum depth we observe today in Mikumi crater is just around 500 m.

4.1. Morpho-stratigraphic mapping

In order to study the stratigraphic relationship between the clay and sulfate units exposed within Mikumi crater we performed a morpho-stratigraphic mapping of the crater floor at 1:10,000 scale, using CTX data as a basemap, and CRISM and HiRISE datasets for additional information on composition and morphology, respectively. The map is shown in Fig. 5, along with a cross-section and a stratigraphic column. The main mapped units are described in detail below:

4.1.1. Description of the mapped units

(a) **Bottom floor unit (bfu)** - Fig. 6a: meter-scale pitted bright bedrock where several layers are observed. This unit is mostly covered by dunes with star shape. Unknown bedrock composition due to the dune covering and possibly dust (Figure S9).

(b) **Sulfate unit A (suA)** - Fig. 6b: layered monohydrated sulfate unit, always covered by a thin layer of loose material which masks most of its morphological surface features.

(c) **Sulfate unit B (suB)** - Fig. 6b and c: very bright and layered unit, rich in polyhydrated sulfates. Easily erodible: erosional features such as mesas are the

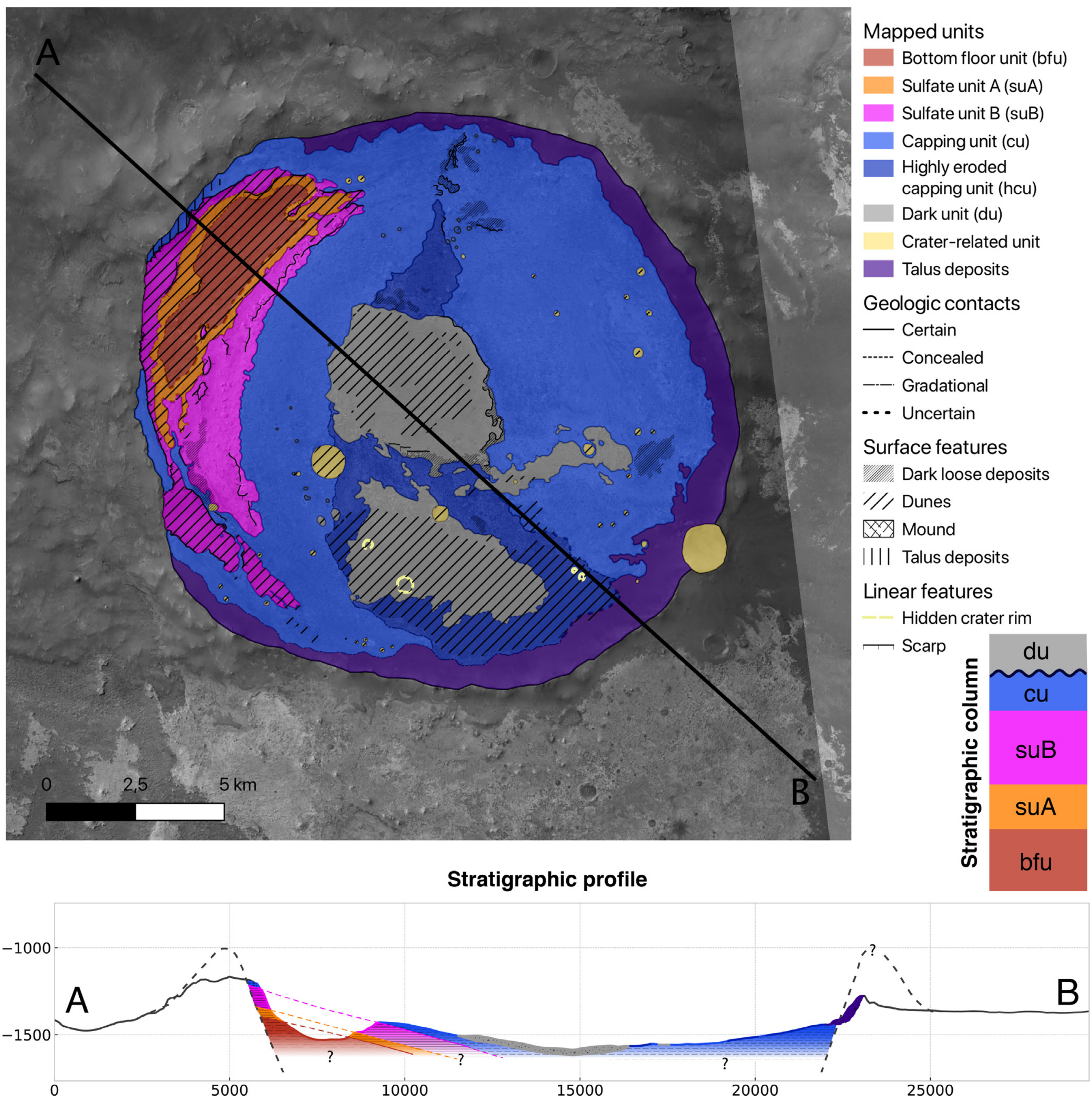

Fig. 5. 1:10,000 Morpho-stratigraphic map of Mikumi crater. A detailed description of the main units can be found in Section 4.1. A stratigraphic column and a stratigraphic profile (5x vertical exaggeration) are also shown here. Black solid line in the profile shows current topography, while dashed line shows the possible crater rim before degradation, colourful dashed lines connect the same units on each side of the topographic low in the western part of the crater floor. For further details about the stratigraphy refer to Section 4.2.

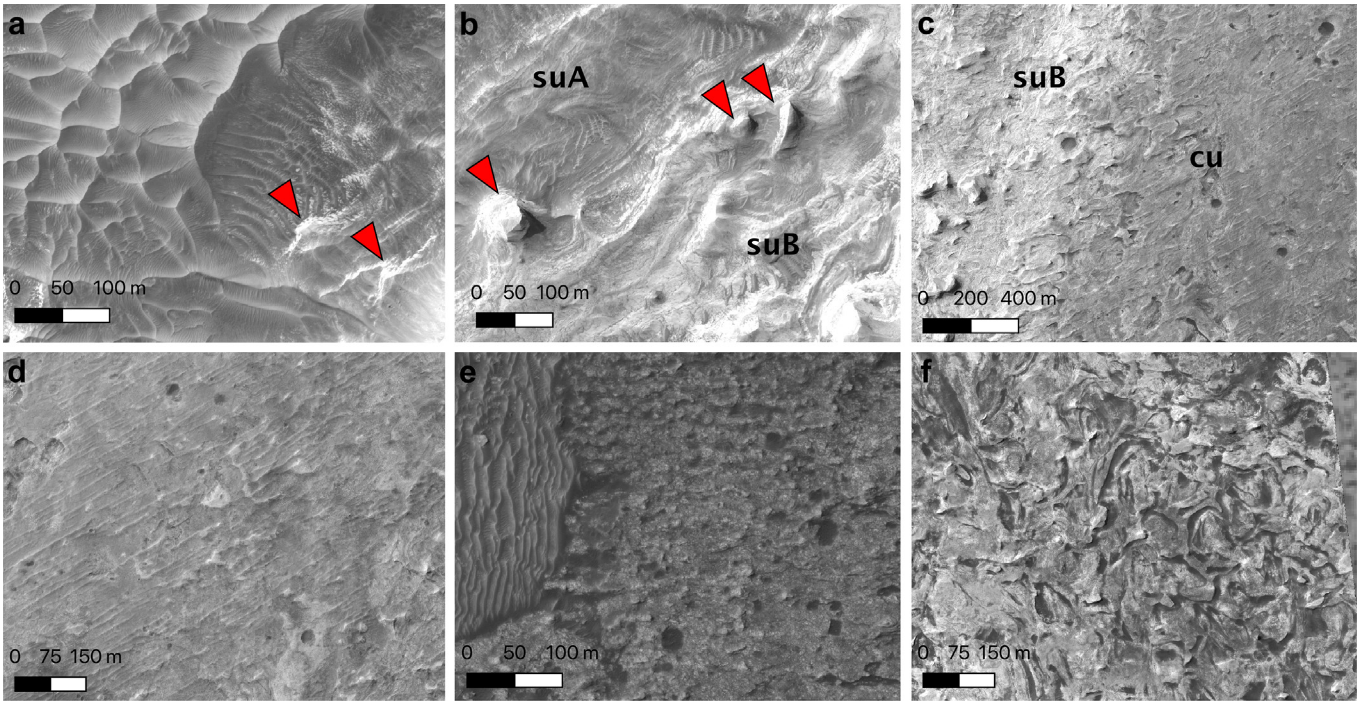

Fig. 6. Description of mapped units from Fig. 5. (a) Bottom floor unit (bfu). This unit is a bright layered unit showing some pitted morphology (some of the layers are pointed out with red arrows). It is almost completely covered by star dunes (left part of the image). (b) Boundary between sulfate unit A (suA), and sulfate unit B (suB). suA surface characteristics are not clear: it appears covered by loose materials which mask its morphological features. suB is bright and highly erodible, several mesas are visible. (c) Boundary between sulfate unit B (suB) and the Fe/Mg phyllosilicate-rich capping unit (cu). Note the change in albedo. cu has an intermediate albedo and is generally smooth with sometimes thin ridges oriented SW to NE (Fig. 6d). cu surface is also extensively polygonally patterned (see Figs. 8 and 9). (d) Capping unit (cu) surface characteristics. SW-NE oriented ridges are visible over some areas. More details on the texture are discussed in Section 4.3. (e) Dark unit (du). This unit is a dark and rough unit which is covered in some areas by large dune fields (left part of the image). (f) Highly eroded capping unit (hcu). This unit is characterised by complex erosional features.

most evident characteristics (Fig. 6b). This unit is also mildly fractured, with loose darker materials accumulating in the fractures.

(d) **Capping unit (cu) -** Fig. 6c and d: intermediate albedo, generally flat and extensively polygonally patterned. Layers and scarps are visible on this unit in the northern part of the crater. SW-NE oriented thin bright ridges are visible in some areas, especially on the western part, close to suB. Spectral data show that this unit is rich in Fe/Mg phyllosilicates. We observe different areas within cu, which vary in terms of relative Fe/Mg content of the phyllosilicates and show some changes in the texture of the terrains. The scale we chose for our map is too small to distinguish between them but more details on the correlation between texture and clay mineralogy are discussed in Section 4.3.

(e) **Highly eroded capping unit (hcu) -** Fig. 6f: this unit can be associated to the geologic unit cu but having undergone intense erosion. Surface features are extremely complex and irregular, with several elongated depressions. Where coverage is available, CRISM data show signs of hydration (Fe/Mg phyllosilicates) throughout this unit.

(f) **Dark unit (du) -** Fig. 6e: low albedo and rough texture. Some areas are covered by large dune fields. Unit boundaries are generally sharp and clear. Unknown composition.

4.2. Stratigraphy

Most of the mapped units inside Mikumi's floor are exposed below the long scarp in the western part of the crater. In particular, here we can clearly assess the stratigraphic relationship between bfu, suA, suB and cu/hcu (Fig. 7).

The oldest exposed unit is bfu, which is overlied by suA (monohydrated sulfates), and then suB (polyhydrated sulfates). These three units share similar characteristics: all three units are layered, both bfu and suB have high albedo, and both suA and suB are sulfate rich. The overall thickness of the sulfate sequence (suA + suB) is around 75 metres. suB is then capped by cu/hcu, which is thinner (thickness varies between 15 and 40 meters, and is about 20–30 m on average) and rich in Fe/Mg phyllosilicates. Based on plane fitting using the CTX digital elevation model of the area, it seems that the materials inside

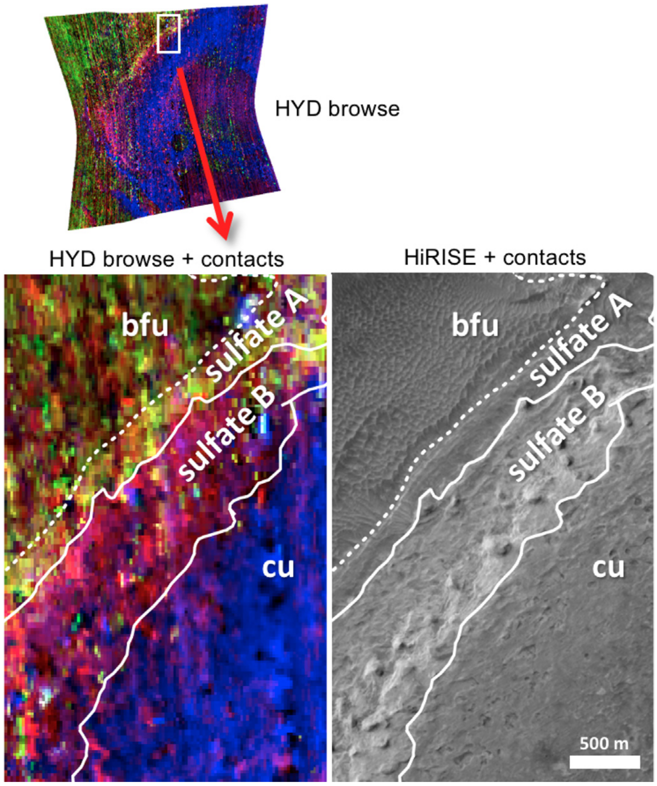

Fig. 7. Contacts between the mapped units along the scarp in the western part of Mikumi crater. The solid line marks certain contacts, while the dashed line marks uncertain contacts.

Mikumi crater were deposited almost horizontally, with a slight tilt towards S/SE (about 4.5 degrees on average). Moreover, we do not observe unconformities in the bfu-suA-suB-cu sequence. Finally, the youngest unit is du, which unconformably overlays cu/hcu and is found on the central and southern part of the crater. Where visible, contacts between cu/hcu and du are very sharp. The above information is summarised in a stratigraphic column and in a stratigraphic profile (see Fig. 5).

4.3. Correlation between Fe/Mg phyllosilicates distribution and texture

In this section we discuss more in detail some characteristics of the capping unit (cu), describing its small-scale textural variations in relation with the Fe/Mg content of the phyllosilicates in the area.

Some of the regions with a higher concentration of Fe-enriched smectites (Fig. 2b) are found close to the southern rim of Mikumi crater (Fig. 8A, S4 and S6), surrounding a smaller crater (<1 km) SW to the central du unit (Fig. 8B S5 and S6), and on a group of terrains located in the northern part of the crater. The exact locations for Fig. 8A and B are shown by red outlines, labeled A and B, in the upper right panel of Fig. 8. All these areas are generally bright and polygonally patterned in most parts. There is a good correlation between the texture of the terrains and the strength of the Fe-enriched smectites detection. The stronger the detection, the rougher the texture of the terrains, with highly contrasted polygons (See enlargements i, ii, and iii of Fig. 8). As we move from areas with smectites richer in Fe, towards areas with smectites richer in Mg, the terrains appear smoother and the polygons are less contrasted. Polygons also vary in size, Fig. 9 shows the area northwest of the small crater in Fig. 8B (exact location is shown by red outline C, in the upper right panel of the figure), where smectites richer in magnesium are detected as the most abundant mineralogy. In these regions we observe bright areas with smaller polygons (< 1 m or ∼1–2 m in size), similar to the ones found in Fe-enriched terrains, interrupted by darker areas with bigger polygonal structures (of about 5–10 m in size, see red arrows in enlargement i of Fig. 9).

5. Discussion

As we have seen in Section 3, our analysis has evidenced the presence of low-Ca pyroxenes in the areas of the crater's rim, and Fe/Mg-rich phyllosilicates and sulfates on a wide part of the floor. The pyroxenes detected probably reflect the general composition of the bedrock in the area, which is indeed dominated by low-calcium and high-calcium pyroxenes (e.g. Poulet et al., 2008; Griffes et al., 2007). Fe/Mg phyllosilicates and sulfates compose the sediments which fill the crater's floor, consistently with the detection of hydrated materials in northern Meridiani Planum, especially inside craters (Poulet et al., 2008; Flahaut et al., 2015; Wiseman et al., 2010). In addition, in this study we provide a deeper insight into the characteristics of these materials and their stratigraphic relationship.

Fe/Mg phyllosilicates are detected on a geological unit which has varying morphological characteristics correlating with changes in the Fe/Mg content of the clays. Tens of meters of mono- and polyhydrated sulfates are also detected below this clay-rich unit, further enriching the mineralogical diversity within this small crater. In the next sections we will discuss in detail the implications for the observed stratigraphy, some possible formation mechanisms for the polygons, and the possible sequence of events which led to the formation of the units within the crater.

5.1. Stratigraphy of the sulfate and clay units

The stratigraphic analysis performed on the clay and sulfate deposits inside Mikumi crater shows that here a layered Fe/Mg phyllosilicate unit (20–30 metres on average) overlies two distinct tens-of-meters-thick layered Mg sulfate units (about 75 metres overall). The oldest of the two sulfate units is composed of monohydrated Mg sulfates (kieserite), while the youngest is made of polyhydrated Mg sulfates. As stated in the results section, all the units inside Mikumi crater are layered and deposited almost horizontally, with just a small tilt of about 4.5 degrees on average, towards S/SE. The existence of this

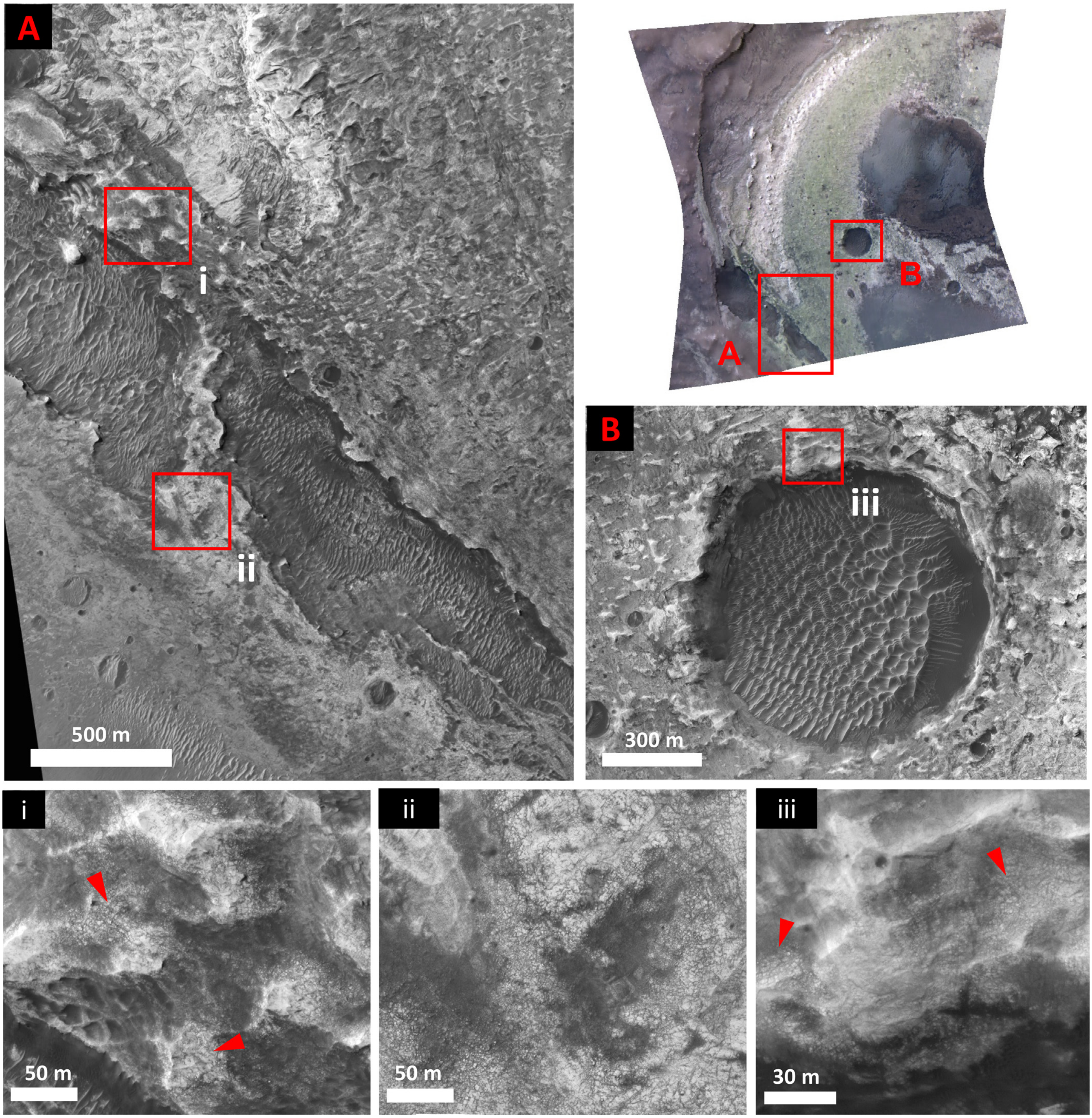

Fig. 8. HiRISE (PSP_009510_1825_RED) close-ups of the crater floor corresponding to some of the areas which show presence of Fe-enriched smectites. For context, panel on the upper right part of the composition shows the CRISM enhanced infrared browse product covering the western part of Mikumi crater. Red outlines indicate the locations of panels A and B. (A) Terrains close to the southern rim of the crater. Note the bright areas with high-contrast polygonal patterns (enlargements i and ii); (B) small crater within the main crater floor. Polygonal patterns are found again close to the crater rim (for example, as indicated by the red arrows in enlargement iii).

well-defined and well-preserved sulfate/clay sequence within Mikumi crater is indicative of deposition events that must have taken place after the crater formation. In particular, the absence of unconformities at the contacts between suA and suB units, and between suB and cu, suggest a coherent stratigraphic succession in which sulfates formed before the clays were emplaced. This indicates a more complex sequence of events in comparison to what, for example, Wiseman et al. (2010) suggested for this area, where Fe/Mg phyllosilicates were detected only on terrains which predated the sulfate-rich units mapped in their study. Alternative explanations for the physical collocation of the sulfate layers below the clay unit, such as the action of groundwater flows that could have: (a) dissolved and

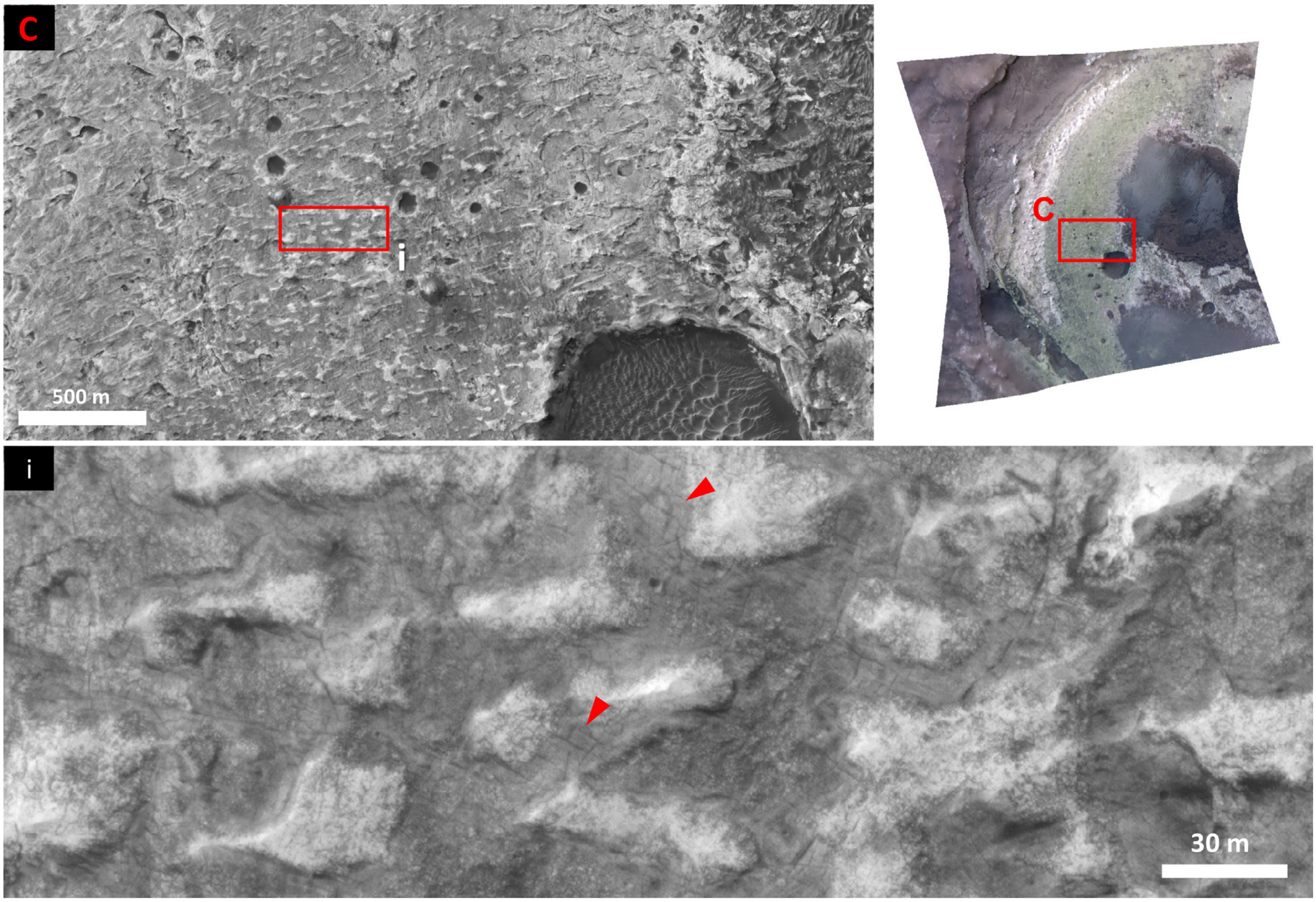

Fig. 9. HiRISE (PSP_009510_1825_RED) close-up of the crater floor corresponding to areas which show the presence of Mg-enriched smectites. For context, panel on the upper right part of the composition shows the CRISM enhanced infrared browse product covering the western part of Mikumi crater. Red outlines indicate the location of panel C. Bright terrains with smaller polygons alternate to darker terrains with bigger polygons (for example, see red arrows in enlargement i).

remobilized an upper sulfate layer moving it stratigraphically lower than the clays; (b) infiltrated acidic fluids from the bottom of the clay unit, altering the clays at depth and forming the sulfates (e.g. Altheide et al., 2010); are highly unlikely in our case. Case (a) does not explain the preservation of the clay-layer: it is quite unexpected that the layer would remain intact during the sulfate remobilization. Moreover, it is also important to bear in mind the huge thickness of the sulfate units. Such thickness greatly limits the amount of reasonable formation mechanisms. In particular, on Earth similar or greater thicknesses of sulfates are associated with ancient marine-fed systems and some endorheic basins (Warren, 2010), where salts precipitate from supersaturated aqueous solutions. This evidence alone tends to exclude both option (a) and (b) as the processes involved there would not be able to form ~75-meter-tick sulfate-bearing deposits. Even assuming those mechanisms could be able to form tens of meters of sulfates, the formation/remobilization of such amounts of salts after the clay deposition would have created huge deformations in the clay layer, which we do not observe.

5.2. Paleoenvironmental significance of the clay and sulfate mineralogies

For a long time, the presence of Fe/Mg clays on the surface of Mars has been considered exclusive to exposures of Noachian materials, while sulfates were typically found as a common alteration product on Hesperian surfaces (Bibring et al., 2006; Murchie et al., 2007). Due to the different ages and chemistry of the deposits of these secondary minerals, Bibring et al. (2006) suggested that the presence of one rather than the other could be a significant marker of different genetic environments. Phyllosilicate formation was favoured by water-rich near neutral to alkaline conditions ($6<pH<12$) common during the Noachian, while sulfate formation was favoured under the drier and more acidic conditions of the Hesperian epoch. More recently, newer studies have started to point out that clays can co-occur with sulfates, for example as observed with both orbital and in situ measurements in part of the stratigraphic sequence of the Late Noachian-Early Hesperian Mount Sharp, in Gale crater (e.g. Sheppard et al., 2021a;

Sheppard et al., 2021b); and that surface conditions favourable to clays may have been present, at least locally, even in the Hesperian (Sun and Milliken, 2014). For this reason, a linear clay-to-sulfate trend, which was associated to the transition of Mars' environment from wet to dry, is now being recognised as an oversimplified interpretation of the planet's past aqueous activity. The necessity of a change of paradigm also seems to be required to explain some recent non-mineralogical in situ observations such as those reported at Gale crater by Rapin et al. (2021). The results of this work show that in Mikumi crater thick (~75 m) sulfate-bearing deposits are conformably overlain by 20–30 meters, on average, of Fe/Mg phyllosilicate-rich deposits (Figs. 5 and 7), meaning that sulfates observed here are older than clays, providing yet another proof of this oversimplification. A similar sequence to the one shown in this study has also been observed in other areas of Meridiani Planum by Flahaut et al. (2015). Specifically, the authors observed a sulfate/clay/sulfate succession across the Noachian–Hesperian etched terrains south to Mikumi crater. These observations could be related to the sequence we observe in this study. However, more work is needed to assess the exact stratigraphic relationship between these two areas.

The observed stratigraphic sequence of the sulfate and clay units within Mikumi crater is showing a transition between an environment which favours abundant sulfate deposition to one that favours the formation of Fe/Mg clays. The units are then classified by Hynek et al. (2017) as part of the etched units of Meridiani Planum (HNMeu), which were deposited during the Late Noachian/Early Hesperian epochs. This could imply that, approaching the Noachian–Hesperian boundary, the climate of Mars experienced some oscillations, with dryer periods favouring sulfate deposition followed by wetter periods favouring clay formation. A part of the timing and characteristics of these oscillations are recorded in the stratigraphy of Mikumi crater and probably in other areas of Meridiani Planum as well, which makes this region a very valuable study case for paleoenvironmental and paleoclimatic studies of Mars. However, it is still possible that peculiar water-related events occurred locally in Meridiani Planum, leading to the formation of sulfates before the clay emplacement. It is therefore important to look for, study and correlate similar sequences elsewhere on Mars.

Finally, it is worth mentioning here that some spectral characteristics, such as the intensity of the spectral signature of a certain unit, can also be driven by non-compositional factors. For example, in the case of the Glen Torridon in Gale crater, Dehouck et al. (2022) highlights how, despite CRISM data in this area show strong clay signatures, in situ investigations by Curiosity demonstrated that the unit did not experience significantly greater aqueous alteration than other units previously investigated by the rover (which exhibited fainter clay signatures). It is therefore a delicate matter to discuss climatic interpretations based on orbital spectroscopic data alone. For this reason, our climatic interpretation does not rely on any abundance estimation of the observed clay and sulfate mineralogy, and it also takes into consideration other factors such as the thickness of the units and their morphological context.

5.3. Origin of the polygons

Terrains associated with either Fe/Mg phyllosilicates or Mg sulfates show different types of polygonal patterns, as seen in Section 4. Trying to understand the formation mechanism of these patterns relying solely on remotely sensed images is a challenging task. Several kinds of processes could account for similar features and it's difficult to completely rule out one option with respect to the other. Based on photo evidence from several authors (e.g. Loizeau et al., 2007; El-Maarry et al., 2014; Flahaut et al., 2015) showing features in Meridiani Planum and elsewhere on Mars that look very close to what we observe here, in this section we discuss the possibility that the polygonal texture on our terrains might be created by fracture patterns running through the surface. Some possible explanations for the overall formation of these cracks might be related for example to desiccation processes, thermal contraction or hydraulic fracturing.

Desiccation is caused by water evaporation or migration: as a result of the water loss, the terrain shrinks and cracks. Fracture patterns which may be related to desiccation are found in various Martian terrains and are usually associated with sedimentary environments and the detection of Fe/Mg smectites, Al-smectites, less commonly kaolinites, carbonates, and sulfates (El-Maarry et al., 2014, and references therein). Closed basins, including crater floors, are the typical morphological setting of desiccation cracks (e.g. Ehlmann et al., 2008). In Meridiani Planum, based on observations by Opportunity rover, Amundson (2018) reports the presence of cracks and polygonal structures in sulfate-rich areas suggesting that they are the consequence of multiple wetting and drying cycles. Thermal contraction on Mars (e.g. Levy et al., 2009; Lefort et al., 2010) is usually a latitude-dependent mechanism (generally happening at latitudes greater than 45°), where ice-rich terrains crack as a result of temperature variations. While open, soil and other detritus fall into the crack, preventing it from completely healing when thawed, therefore, the crack is likely to open again with the next winter (Goehring, 2013). The morphology and evolution of the patterns due to seasonal thermal variations are similar to desiccation cracks evolving with multiple wetting and drying events (Goehring, 2013). These cracks occur on all types of terrains, they do not show a preference for basins and also occur on plains and slopes (Levy et al., 2009, and references therein). Finally, hydraulic fractures form as a result of elevated fluid pressure in buried sediments. Fractures formed by hydraulic fracturing are well documented for example in Gale crater (e.g. Caswell and Milliken, 2017; Kronyak et al., 2019). Additionally, hydraulic fracturing is a possible hypothesis for the fractured clay-bearing units observed in Oxia Planum (Quantin-Nataf et al., 2021).

Given the regional context evidencing widespread surface and near-surface aqueous activity, the presence of a thick sequence of sediments with hydrous mineralogy, and the basin environment (although no inlets or outlets are observed), we think that a combination of desiccation and hydraulic fracturing processes might have acted on the sediments inside Mikumi crater. Specifically, hydraulic fracturing could have been the major process responsible for the cracks we observe on the sulfate sediments, as these form a very thick sequence that may have experienced elevated fluid pressure due to overlying layers, included the capping clay layer. Desiccation could then be the main fracturing process on this last, more surficial, layer. Thermal contraction is usually associated with higher latitudes, while Mikumi crater is very close to the Martian equator. However, we cannot exclude this hypothesis when considering the possibility of changes in obliquity of the planet during the past (e.g. Head et al., 2003). As we pointed out in Section 4.3, polygons on the capping unit vary in size and terrains show different characteristics, which seem to correlate with the variation in the Fe/Mg content of the phyllosilicates. We are not sure about what could cause this differentiation and the different mineralogy might be just one of the possible reasons. This might also involve a different thickness of the layers of sediments or different formation conditions.

5.4. Proposed sequence of events

Mikumi crater formed on the Noachian bedrock of Meridiani Planum (Nhc1 unit, see Fig. 1), which is now exposed mainly in the northern part of the region and is greatly dissected by several types of channels and valley networks (Williams et al., 2017), implying the existence of an early, pre-impact, aqueous period in the region. Since its formation, the crater, whose diameter implies an original depth between 2.2 and 3.6 km (Mouginis-Mark et al., 2018), has been infilled by sediments up to the actual depth of around 450–500 m. Only a small part of these material is now exposed in the crater, mainly on a scarp running around the topographic low in the eastern part of the crater floor. Unfortunately, we can only probe the composition and study the morphological expression of the most surficial layers of the sequence, which are less than 100 m overall. For the first part of the exposed sequence, which is sulfate-rich, precipitation in a standing body of water is the formation mechanism which can more likely account for the observed thickness. Similar extents of sulfate evaporites are usually found on Earth as a result of the evaporation of supersaturated waters in endorheic basins and ancient marine-fed systems (e.g. Warren, 2010; Bastow et al., 2018), where topographic conditions do not allow the outflow of water and climate is relatively dry for a prolonged period of time. As discussed in Section 5.1, it is more challenging that fluid circulation in a pre-existing sediment could account for the amount of sulfates observed here, although we don't exclude that this could have contributed to the observed thickness. Currently, differentiation between monohydrated and polyhydrated sulfates, which sedimented in stratigraphic succession, remains elusive and debated (e.g. Roach et al., 2009; Wang et al., 2016). Clays were then deposited in a conformable succession on the sulfate sequence. The absence of fluvial transport features, such as inlets, outlets and deltas in Mikumi crater argue against an aqueous transportation origin for this unit. While non-aqueous transportation is still possible, we do not observe obvious sources of clay-rich sediments nearby. For these reasons, clay minerals may have formed in situ, either from direct precipitation from a standing body of water or from alteration of a previously emplaced sedimentary unit. In any case, the chemical composition of the water involved is expected to be different from the one which formed the sulfates, since clay formation is generally favoured in neutral-alkaline waters. Prior to the deposition of the dark unit (du), the area underwent a period of extensive erosion that exposed the sulfates in the western part of the crater. Finally, du itself shows varying degrees of erosion. Although we do not have clear spectral information on the composition of the dark unit, it is probably mafic in nature, similar to covering units observed in other parts of Meridiani and Arabia Terra. This is usually interpreted as the residue of a volcanic deposit, lava or pyroclastic, and to date it is observed only in the central part of the crater. Regarding the volcanic origin, this could imply lava flows from nearby springs (Head et al., 2002; Pan et al., 2017; Quantin-Nataf et al., 2021) or volcanic ash, altered and lithified, from nearby calderas or volcanic chimneys (Michalski and Bleacher, 2013; Whelley et al., 2021). Today, the area is dominated by aeolian processes, as evidenced by the dust and dune fields widely present in the topographic lows of the crater floor. The sequence of events described in this paragraph has been summarised in Fig. 10.

The aqueous processes involved in the formation of the sulfate and clay units in Mikumi crater add a layer of complexity to the geologic history of Meridiani Planum. Previous studies of this area, particularly in situ data and interpretations by Opportunity, indicate several events of water circulation and alteration in Meridiani units (e.g. Crumpler et al., 2015). In particular, at the rim of Endeavour crater, the rover characterized the outcrop known as Matijevic formation. This is the oldest unit observed by Opportunity during its traverse, formed by clay-rich Noachian materials pre-dating the formation of Endeavour impact crater (Arvidson et al., 2014; Crumpler et al., 2015). The youngest unit observed corresponds instead to the sulfate-cemented sandstone of the Burns formation (e.g. Squyres and Knoll, 2005; Grotzinger et al., 2005). Despite the similar mineralogy, the history of formation of these deposits appears different from what we observe in Mikumi crater, where both suA/suB (sulfate-rich) and

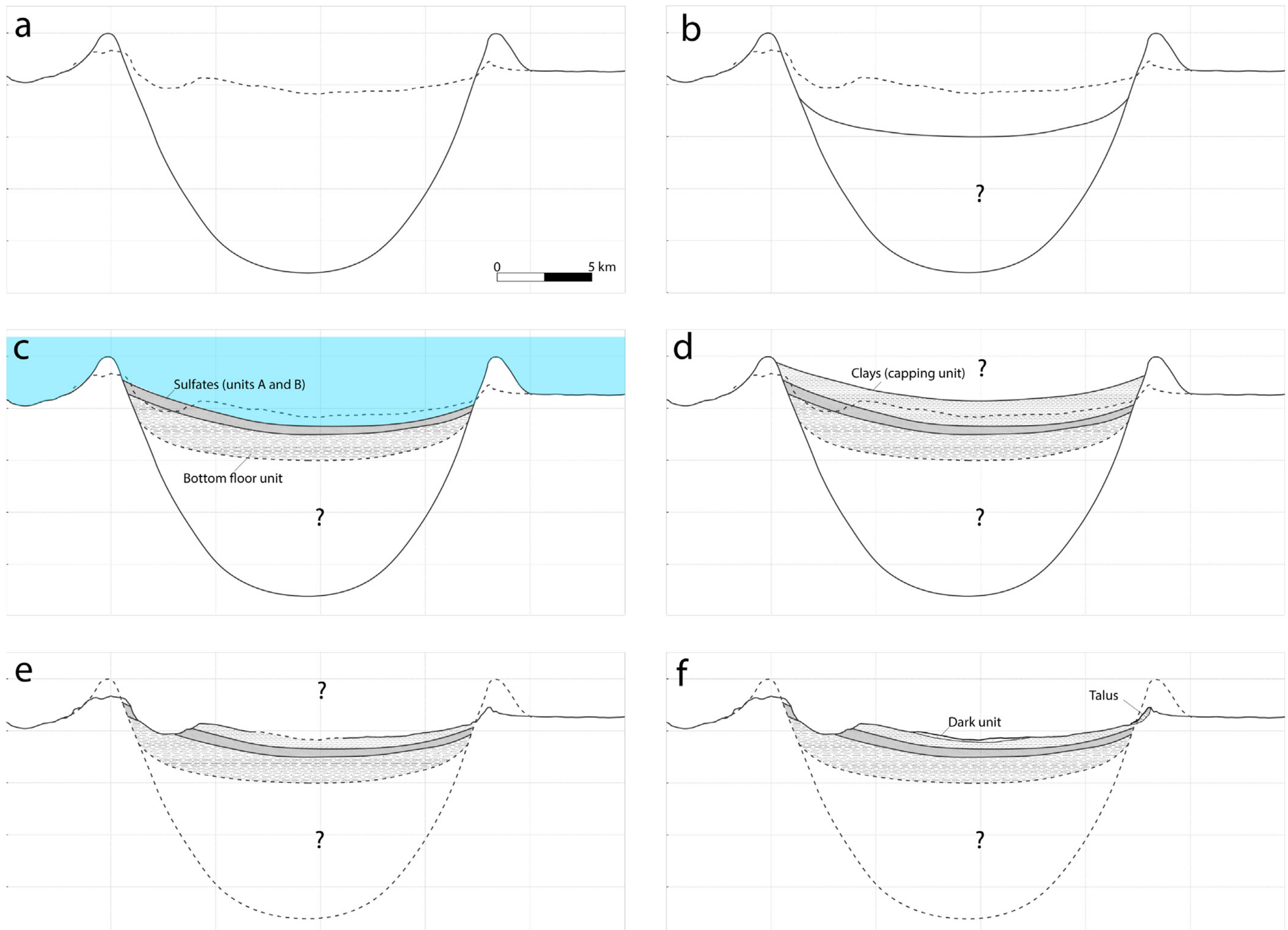

Fig. 10. Proposed sequence of events for the infilling of Mikumi crater. Simplification of the section shown in Fig. 5, with 5x vertical exaggeration. In a-d supposed original crater topography is shown with a solid line (current topography is dashed) as reconstructed with estimations based on d_t/D measurements (Section 4). In e-f, post-erosion, the symbols of the lines are reversed. (a) Formation of Mikumi crater. (b) Infilling of the crater by unknown sediments. (c) Formation of the bottom floor unit and precipitation of the sulfate units (suA + suB) in a standing body of water for a prolonged period of time. The reported water level is merely indicative and not clearly measurable by the available data. However, the choice to place the water level outside the crater is due to evidence, as indicated in regional works such as (Flahaut et al., 2015), which highlight the presence of several sulfate-rich intracrater deposits. This makes such a scenario plausible. (d) Deposition of the clay-rich capping unit. (e) Erosion of the capping unit and exhumation of the sulfate units underneath. (f) Deposition and subsequent erosion of the dark unit, emplacement of aeolian and talus deposits.

cu (clay-rich) units were emplaced after the crater formation, in the opposite stratigraphic order and with cu conformably overlying the sulfate units. There is also no evidence of tectonic-structural phenomena that could have overturned the original stratigraphic sequence at Mikumi. The clays we observe in Mikumi crater cannot belong to the Noachian units of Meridiani and are therefore not related to those found in the Matijevic formation. As a result, the aqueous activity recorded by Opportunity is not representative of the whole history of water alteration at Meridiani Planum.

6. Conclusions

Mikumi crater is a 16-km-wide crater located in the northern part of Meridiani Planum whose floor is filled by sedimentary rocks showing a rich and varied hydrated mineralogy. Fe/Mg phyllosilicates, along with monohydrated and polyhydrated sulfates (kieserite and Mg sulfate), are detected on the crater floor, while the crater rim and the areas directly outside it show a mafic composition with predominance of low-Ca pyroxenes, reflecting the general bedrock composition of the region. The polyhydrated sulfate and the Fe/Mg phyllosilicate units are polygonally fractured, probably due to a mix of desiccation and hydro fracturing processes. Additionally, Fe/Mg phyllosilicates show a certain degree of diversity in their Fe and Mg content throughout the unit which seem to correlate with changes in fracture sizes.

The sedimentary rocks that fill Mikumi crater, which are interpreted by (Hynek et al., 2017) as being deposited between the Late Noachian and Early Hesperian, show a stratigraphic succession where phyllosilicates were conformably deposited on top of two distinct thick sulfate units (a monohydrated sulfate unit overlain by a polyhydrated sulfate unit which have an overall thickness of about 75 metres), meaning that the first formed later than the other two. This has interesting implication in terms of paleoenvironmental and paleoclimatic investigations on Mars as it doesn't follow the trend traditionally expected for the planet on a global scale (Bibring et al., 2006). Sulfates and clays are typically related to different epochs of the Martian history and usually form under different environmental conditions. In particular, clays are abundant on Noachian surfaces, while sulfates are abundant on Hesperian ones (e.g. Bibring et al., 2006). However, the stratigraphic succession of the phyllosilicate and sulfate units observed in Mikumi crater shows that a simple timeline going from a clay-rich Noachian to a sulfate-rich Hesperian is an oversimplified view, which can't completely explain the evolution of Mars' mineralogy and its related aqueous environments, especially at the Noachian–Hesperian boundary. The results of this study support other recent results which suggest that the temporal and spatial division between clay- and sulfate-forming environments, or more generally between wet and dryer environments, inferred from a global view, is more complex than previously thought or does not apply in some cases (e.g. Rapin et al., 2021; Sheppard et al., 2021a; Sun and Milliken, 2014).

Further investigation is needed to assess if the monohydrated sulfate/polyhydrated sulfate/clay stratigraphic sequence we find in Mikumi crater can be observed further north in the area and what is its relationship with southern areas of Meridiani Planum, where a sulfate/clay/sulfate sequence is reported by Flahaut et al. (2015). However, we show here that Mikumi crater is a very interesting site in Meridiani Planum as the thick sequence of sedimentary rocks we find here can provide a great deal of information about paleoenvironmental characteristics and variabilities. For this reason, Mikumi can also be an interesting site where to land on Mars with future missions. The characteristics of the Noachian–Hesperian climatic transition and in general of Mars' early climate are still unclear and highly debated and in situ analysis in this key area could help shed light on that crucial epoch of Mars history.

Declaration of Competing Interest

The authors declare that they have no known competing financial interests or personal relationships that could have appeared to influence the work reported in this paper.

Acknowledgments

We thank Matteo Massironi and Anna Breda for useful advice and discussion on the results. We also kindly thank the three anonymous reviewers for their comments and suggestions, which greatly improved this manuscript. The morpho-stratigraphic map shown in this article was produced with the help of the "Mappy" plugin for QGIS. This project was partially funded by Europlanet RI20-24 GMAP project (research grant agreement No. 871149-GMAP).

Appendix A. Supplementary material

Supplementary data associated with this article can be found, in the online version, at https://doi.org/10.1016/j.asr.2023.12.060.

References

Altheide, T.S., Chevrier, V.F., Noe Dobrea, E., 2010. Mineralogical characterization of acid weathered phyllosilicates with implications for secondary martian deposits. Geochim. Cosmochim. Acta 74 (21), 6232–6248. https://doi.org/10.1016/j.gca.2010.08.005.

Amundson, R., 2018. Meteoric water alteration of soil and landscapes at Meridiani Planum, Mars. Earth Planet. Sci. Lett. 488, 155–167. https://doi.org/10.1016/j.epsl.2018.02.012.

Arvidson, R.E., Poulet, F., Morris, R.V. et al., 2006. Nature and origin of the hematite-bearing plains of terra meridiani based on analyses of orbital and mars exploration rover data sets. J. Geophys. Res. (Planets), 111(E12), E12S08. URL: https://ui.adsabs.harvard.edu/abs/2006JGRE.11112S08A. doi:10.1029/2006JE002728.

Arvidson, R.E., Seelos IV, F.P., Deal, K.S., et al., 2003. Mantled and exhumed terrains in terra meridiani, mars. J. Geophys. Res.: Planets 108 (E12). https://doi.org/10.1029/2002JE001982.

Arvidson, R.E., Squyres, S.W., Bell, J.F., et al., 2014. Ancient aqueous environments at endeavour crater. Mars. Sci. 343 (6169), 1248097. https://doi.org/10.1126/science.1248097.

Baioni, D., & Sgavetti, M., 2013. Karst terrains as possible lithologic and stratigraphic markers in northern sinus meridiani, mars. Planetary and Space Science, 75, 173–181. URL: https://www.sciencedirect.com/science/article/pii/S0032063312002486. doi: 10.1016/j.pss.2012.08.011.

Bastow, I.D., Booth, A.D., Corti, G., et al., 2018. The Development of Late-Stage Continental Breakup: Seismic Reflection and Borehole Evidence from the Danakil Depression. Ethiopia. Tectonics 37 (9), 2848–2862. https://doi.org/10.1029/2017TC004798.

Bibring, J.-P., Langevin, Y., Mustard, J.F., et al., 2006. Global Mineralogical and Aqueous Mars History Derived from OMEGA/Mars Express Data. Science 312 (5772), 400–404. https://doi.org/10.1126/science.1122659.

Burns, R.G. (1993). Mineralogical Applications of Crystal Field Theory.

Caswell, T.E., Milliken, R.E., 2017. Evidence for hydraulic fracturing at Gale crater, Mars: Implications for burial depth of the Yellowknife Bay formation. Earth Planet. Sci. Lett. 468, 72–84. https://doi.org/10.1016/j.epsl.2017.03.033.

Christensen, P.R., Morris, R.V., Lane, M.D. et al., 2001. Global mapping of martian hematite mineral deposits: Remnants of water-driven processes on early mars. J. Geophys. Res., 106(E10), 23873–23886. URL: https://ui.adsabs.harvard.edu/abs/2001JGR...10623873C. doi:10.1029/2000JE001415.

Clark, B.C., Morris, R.V., McLennan, S.M. et al., 2005. Chemistry and mineralogy of outcrops at meridiani planum. Earth and Planet. Sci. Lett., 240(1), 73–94. URL: https://ui.adsabs.harvard.edu/abs/2005E&PSL.240...73C. doi:10.1016/j.epsl.2005.09.040.

Clark, R.N., King, T.V.V., Klejwa, M., et al., 1990. High spectral resolution reflectance spectroscopy of minerals. J. Geophys. Res. 95, 12653–12680. https://doi.org/10.1029/JB095iB08p12653.

Clark, R.N. et al. (1999). Spectroscopy of rocks and minerals, and principles of spectroscopy volume 3.

Cloutis, E.A., Gaffey, M.J., 1991. Pyroxene spectroscopy revisited - Spectral-compositional correlations and relationship to geothermometry. J. Geophys. Res. 96, 22809–22826. https://doi.org/10.1029/91JE02512.

Cloutis, E.A., Hawthorne, F.C., Mertzman, S.A., et al., 2006. Detection and discrimination of sulfate minerals using reflectance spectroscopy. Icarus 184 (1), 121–157. https://doi.org/10.1016/j.icarus.2006.04.003.

Crumpler, L.S., Arvidson, R.E., Bell, J., et al., 2015. Context of ancient aqueous environments on Mars from in situ geologic mapping at Endeavour Crater. J. Geophys. Res. (Planets) 120 (3), 538–569. https://doi.org/10.1002/2014JE004699.

Dehouck, E., Cousin, A., Mangold, N., et al., 2022. Bedrock Geochemistry and Alteration History of the Clay-Bearing Glen Torridon Region of Gale Crater. Mars. J. Geophys. Res.: (Planets) 127 (12). https://doi.org/10.1029/2021JE007103, e2021JE007103.

Ehlmann, B.L., Mustard, J.F., Fassett, C.I., et al., 2008. Clay minerals in delta deposits and organic preservation potential on Mars. Nat. Geosci. 1 (6), 355–358. https://doi.org/10.1038/ngeo207.

El-Maarry, M.R., Watters, W., McKeown, N.K., et al., 2014. Potential desiccation cracks on Mars: A synthesis from modeling, analogue-field studies, and global observations. Icarus 241, 248–268. https://doi.org/10.1016/j.icarus.2014.06.033.

Flahaut, J., Carter, J., Poulet, F. et al. (2015). Embedded clays and sulfates in meridiani planum, mars. Icarus, 248, 269–288. URL: https://ui.adsabs.harvard.edu/abs/2015Icar. 248.269F. doi:10.1016/j.icarus.2014.10.046.

Goehring, L., 2013. Evolving fracture patterns: columnar joints, mud cracks and polygonal terrain. Philosophical Transactions of the Royal Society of London Series A 371 (2004). https://doi.org/10.1098/rsta.2012.0353, 20120353–20120353. arXiv:1211.6762.

Griffes, J.L., Arvidson, R.E., Poulet, F., et al., 2007. Geologic and spectral mapping of etched terrain deposits in northern Meridiani Planum. J. Geophys. Res. (Planets) 112 (E8), E08S09. https://doi.org/10.1029/2006JE002811.

Grotzinger, J.P., Arvidson, R.E., Bell, J.F., et al., 2005. Stratigraphy and sedimentology of a dry to wet eolian depositional system, Burns formation, Meridiani Planum. Mars. Earth and Planetary Science Letters 240 (1), 11–72. https://doi.org/10.1016/j.epsl.2005.09.039.

Head, J.W., Mustard, J.F., Kreslavsky, M.A., et al., 2003. Recent ice ages on Mars. Nature 426 (6968), 797–802. https://doi.org/10.1038/nature02114.

Head III, J.W., Kreslavsky, M.A., Pratt, S., 2002. Northern lowlands of mars: Evidence for widespread volcanic flooding and tectonic deformation in the hesperian period. J. Geophys. Res.: Planets 107 (E1), 3-1–3-29. https://doi.org/10.1029/2000JE001445.

Hynek, B.M., Beach, M., Hoke, M.R.T., 2010. Updated global map of martian valley networks and implications for climate and hydrologic processes. J. Geophys. Res.: Planets 115 (E9). https://doi.org/10.1029/2009JE003548.

Hynek, B.M., McCollom, T.M., & Szynkiewicz, A. (2019). Sulfur cycling and mass balance at meridiani, mars. Geophys. Res. Lett., 46(21), 11728–11737. URL: https://ui.adsabs.harvard.edu/abs/2019GeoRL.4611728H. doi:10.1029/2019GL085115.

Hynek, M., B., & Di Achille, G. (2017). Geologic map of meridiani planum. U.S. Geological Survey Report, (p. 3356). URL: https://ui.adsabs.harvard.edu/abs/2017USGS.SIM.3356H. doi:10.3133/sim3356.

Isaacson, P.J., Klima, R.L., Sunshine, J.M., et al., 2014. Visible to near-infrared optical properties of pure synthetic olivine across the olivine solid solution. Am. Mineral. 99 (2–3), 467–478. https://doi.org/10.2138/am.2014.4580.

Klima, R.L., Dyar, M.D., Pieters, C.M., 2011. Near-infrared spectra of clinopyroxenes: Effects of calcium content and crystal structure. Planet. Sci. 46 (3), 379–395. https://doi.org/10.1111/j.1945-5100.2010.01158.x.

Klima, R.L., Pieters, C.M., Dyar, M.D., 2007. Spectroscopy of synthetic Mg-Fe pyroxenes I: Spin-allowed and spin-forbidden crystal field bands in the visible and near-infrared. Planet. Sci. 42 (2), 235–253. https://doi.org/10.1111/j.1945-5100.2007.tb00230.x.

Kronyak, R.E., Kah, L.C., Edgett, K.S., et al., 2019. Mineral-Filled Fractures as Indicators of Multigenerational Fluid Flow in the Pahrump Hills Member of the Murray Formation, Gale Crater. Mars. Earth and Space Science 6 (2), 238–265. https://doi.org/10.1029/2018EA000482.

Lefort, A., Russell, P.S., Thomas, N., 2010. Scalloped terrains in the Peneus and Amphitrites Paterae region of Mars as observed by HiRISE. Icarus 205 (1), 259–268. https://doi.org/10.1016/j.icarus.2009.06.005.

Levy, J., Head, J., Marchant, D., 2009. Thermal contraction crack polygons on Mars: Classification, distribution, and climate implications from HiRISE observations. J. Geophys. Res. (Planets) 114 (E1), E01007. https://doi.org/10.1029/2008JE003273.

Loizeau, D., Mangold, N., Poulet, F., et al., 2007. Phyllosilicates in the Mawrth Vallis region of Mars. J. Geophys. Res. (Planets) 112 (E8), E08S08. https://doi.org/10.1029/2006JE002877.

Malin, M.C., Bell, J.F., Cantor, B.A. et al. (2007). Context camera investigation on board the mars reconnaissance orbiter. Journal of Geophysical Research (Planets), 112(E5), E05S04. URL: https://ui.adsabs.harvard.edu/abs/2007JGRE.112.5S04M. doi:10.1029/2006JE002808.

McEwen, A.S., Eliason, E.M., Bergstrom, J.W. et al. (2007). Mars reconnaissance orbiter's high resolution imaging science experiment (hirise). Journal of Geophysical Research (Planets), 112(E5), E05S02. URL: https://ui.adsabs.harvard.edu/abs/2007JGRE.112.5S02M. doi:10.1029/2005JE002605.

McGuire, P.C., Bishop, J.L., Brown, A.J., et al., 2009. An improvement to the volcano-scan algorithm for atmospheric correction of CRISM and OMEGA spectral data. Planet. Space Sci. 57 (7), 809–815. https://doi.org/10.1016/j.pss.2009.03.007, arXiv:0903.3672.

Michalski, J.R., & Bleacher, J.E. (2013). Supervolcanoes within an ancient volcanic province in Arabia Terra, Mars. Nature, 502(7469), 47–52. URL: http://www.nature.com/articles/nature12482. doi:10.1038/nature12482.

Mouginis-Mark, P.J., Boyce, J., Sharpton, V.L., et al., 2018. Determination of Mars crater geometric data: Insights from high-resolution digital elevation models. Planet. Sci. 53 (4), 726–740. https://doi.org/10.1111/maps.12895.

Murchie, S., Arvidson, R., Bedini, P. et al. (2007). Compact reconnaissance imaging spectrometer for mars (crism) on mars reconnaissance orbiter (mro). Journal of Geophysical Research (Planets), 112(E5), E05S03. URL: https://ui.adsabs.harvard.edu/abs/2007JGRE.112.5S03M. doi:10.1029/2006JE002682.

Pan, L., Ehlmann, B.L., Carter, J. et al. (2017). The stratigraphy and history of Mars' northern lowlands through mineralogy of impact craters: A comprehensive survey. J. Geophys. Res.: Planets, 122(9), 1824–1854. Publisher: Wiley Online Library.

Poulet, F., Arvidson, R.E., Gomez, C. et al. (2008). Mineralogy of terra meridiani and western arabia terra from omega/mex and implications for their formation. Icarus, 195(1), 106–130. URL: https://ui.adsabs.harvard.edu/abs/2008Icar. 195.106P. doi:10.1016/j.icarus.2007.11.031.

Quantin-Nataf, C., Carter, J., Mandon, L., et al., 2021. Oxia Planum: The Landing Site for the ExoMars "Rosalind Franklin" Rover Mission: Geological Context and Prelanding Interpretation. Astrobiology 21 (3), 345–366. https://doi.org/10.1089/ast.2019.2191.

Quantin-Nataf, C., Carter, J., Mandon, L., et al., 2021. Oxia Planum: The Landing Site for the ExoMars "Rosalind Franklin" Rover Mission: Geological Context and Prelanding Interpretation. Astrobiology. Mary Ann Liebert Inc, publishers, p. 22. https://doi.org/10.1089/ast.2019.2191, URL: https://www.liebertpub.com/doi/10.1089/ast.2019.2191.

Rapin, W., Dromart, G., Rubin, D., et al., 2021. Alternating wet and dry depositional environments recorded in the stratigraphy of Mount Sharp at Gale crater. Mars. Geology 49 (7), 842–846. https://doi.org/10.1130/G48519.1.

Roach, L.H., Mustard, J.F., Murchie, S.L., et al., 2009. Testing evidence of recent hydration state change in sulfates on mars. J. Geophys. Res.: Planets 114 (E2). https://doi.org/10.1029/2008JE003245.

Sheppard, R.Y., Milliken, R.E., Parente, M. et al. (2021a). Updated Perspectives and Hypotheses on the Mineralogy of Lower Mt. Sharp, Mars, as Seen From Orbit. Journal of Geophysical Research (Planets), 126(2), e06372. doi:10.1029/2020JE006372.

Sheppard, R.Y., Thorpe, M.T., Fraeman, A.A., et al., 2021b. Merging Perspectives on Secondary Minerals on Mars: A Review of Ancient Water-Rock Interactions in Gale Crater Inferred from Orbital and In-Situ Observations. Minerals 11 (9), 986. https://doi.org/10.3390/min11090986.

Squyres, S.W., Arvidson, R.E., Bollen, D. et al. (2006). Overview of the opportunity mars exploration rover mission to meridiani planum: Eagle crater to purgatory ripple. Journal of Geophysical Research (Planets), 111(E12), E12S12. URL: https://ui.adsabs.harvard.edu/abs/2006JGRE.11112S12S. doi:10.1029/2006JE002771.

Squyres, S.W., Grotzinger, J.P., Arvidson, R.E., et al., 2004. In situ evidence for an ancient aqueous environment at meridiani planum, mars. Science 306 (5702), 1709–1714. https://doi.org/10.1126/science.1104559.

Squyres, S.W., Knoll, A.H., 2005. Sedimentary rocks at Meridiani Planum: Origin, diagenesis, and implications for life on Mars. Earth Planet. Sci. Lett. 240 (1), 1–10. https://doi.org/10.1016/j.epsl.2005.09.038.

Sun, V.Z., Milliken, R.E., 2014. The geology and mineralogy of Ritchey crater, Mars: Evidence for post-Noachian clay formation. J. Geophys. Res. (Planets) 119 (4), 810–836. https://doi.org/10.1002/2013JE004602.

Sunshine, J.M., Pieters, C.M., 1998. Determining the composition of olivine from reflectance spectroscopy. J. Geophys. Res. 103 (E6), 13675–13688. https://doi.org/10.1029/98JE01217.

Viviano-Beck, C.E., Seelos, F.P., Murchie, S.L., et al., 2014. Revised CRISM spectral parameters and summary products based on the currently detected mineral diversity on Mars. J. Geophys. Res. (Planets) 119 (6), 1403–1431. https://doi.org/10.1002/2014JE004627.

Wang, A., Jolliff, B.L., Liu, Y., et al., 2016. Setting constraints on the nature and origin of the two major hydrous sulfates on Mars: Monohydrated and polyhydrated sulfates. J. Geophys. Res. (Planets) 121 (4), 678–694. https://doi.org/10.1002/2015JE004889.

Warren, J.K., 2010. Evaporites through time: Tectonic, climatic and eustatic controls in marine and nonmarine deposits. Earth-Sci. Rev. 98 (3), 217–268. https://doi.org/10.1016/j.earscirev.2009.11.004.

Whelley, P., Matiella Novak, A., Richardson, J. et al., 2021. Stratigraphic evidence for early martian explosive volcanism in Arabia Terra. Geophys. Res. Lett., 48(15), e2021GL094109. Publisher: Wiley Online Library.

Williams, R.M.E., Chuang, F.C., Berman, D.C., 2017. Multiple surface wetting events in the greater meridiani planum region, mars: Evidence from valley networks within ancient cratered highlands. Geophys. Res. Lett., 44(4), 1669–1678. URL: https://ui.adsabs.harvard.edu/abs/2017GeoRL.44.1669W. doi:10.1002/2016GL072259.

Wiseman, S.M., Arvidson, R.E., Morris, R.V., et al., 2010. Spectral and stratigraphic mapping of hydrated sulfate and phyllosilicate-bearing deposits in northern sinus meridiani, mars. J. Geophys. Res.: Planets 115 (E7). https://doi.org/10.1029/2009JE003354.

Zabrusky, K., Andrews-Hanna, J.C., Wiseman, S.M., 2012. Reconstructing the distribution and depositional history of the sedimentary deposits of arabia terra, mars. Icarus, 220(2), 311–330. URL: https://ui.adsabs.harvard.edu/abs/2012Icar. 220.311Z. doi:10.1016/j.icarus.2012.05.007.

Zurek, R.W., Smrekar, S.E., 2007. An overview of the mars reconnaissance orbiter (mro) science mission. J. Geophys. Res. (Planets), 112 (E5), E05S01. URL: https://ui.adsabs.harvard.edu/abs/2007JGRE.112.5S01Z. doi:10.1029/2006JE002701.